Charge sensing of few-electron ZnO double quantum dots probed by radio-frequency reflectometry

Kosuke Noro,[1,2,3] Motoya Shinozaki,[4,3] Yusuke Kozuka,[3,4] Koichi Baba,[1,2] Kazuma Matsumura,[1,2] Yoshihiro Fujiwara,[1,2] Takeshi Kumasaka,[4] Atsushi Tsukazaki,[5] Masashi Kawasaki,[5,6] and Tomohiro Otsuka[4,1,2,3,7,6,*]

[1]*Research Institute of Electrical Communication, Tohoku University, 2-1-1 Katahira, Aoba-ku, Sendai 980-8577, Japan*
[2]*Department of Electronic Engineering, Graduate School of Engineering, Tohoku University, 6-6 Aramaki Aza Aoba, Aoba-ku, Sendai 980-0845, Japan*
[3]*Research Center for Materials Nanoarchitechtonics (MANA), National Institute for Material Science (NIMS), 1-2-1 Sengen, Tsukuba 305-0047, Japan*
[4]*WPI Advanced Institute for Materials Research, Tohoku University, 2-1-1 Katahira, Aoba-ku, Sendai 980-8577, Japan*
[5]*Department of Applied Physics and Quantum-Phase Electronics Center (QPEC), University of Tokyo, 7-3-1 Hongo, Bunkyo-ku, Tokyo 113-8656, Japan*
[6]*Center for Emergent Matter Science, RIKEN, 2-1 Hirosawa, Wako, Saitama 351-0198, Japan*
[7]*Center for Science and Innovation in Spintronics, Tohoku University, 2-1-1 Katahira, Aoba-ku, Sendai 980-8577, Japan*

(Dated: May 15, 2026)

Zinc oxide (ZnO) has garnered much attention as a promising material for quantum devices due to its unique characteristics. To utilize the potential of ZnO for quantum devices, the development of fundamental technological elements such as high-speed readout and charge sensing capabilities has become essential. In this study, we address these challenges by demonstrating radio-frequency (rf) reflectometry and charge sensing in ZnO quantum dots, thus advancing the potential for qubit applications. A device is fabricated on a high-quality ZnO heterostructure, featuring gate-defined target and sensor quantum dots. The sensor dot, integrated into an rf resonator circuit, enables the detection of single-electron charges in the target dots. Using this setup, we observe the rf-detected charge stability diagram indicating the formation of few-electron double quantum dots and provide the first benchmark of the bandwidth, sensitivity, and readout fidelity of rf reflectometry.

I. INTRODUCTION

Gate-defined semiconductor quantum dots, called artificial atoms, are representative systems that allow the control of quantum states [1–3]. Few-electron quantum dots are used as quantum bits (qubits), which are the fundamental building blocks of quantum computing [4, 5]. Many efforts have been underway to develop qubits with deeper understanding of materials. In the early stages, gallium arsenide (GaAs) systems were widely used [6, 7] because the technology for forming high-quality two-dimensional electron gases (2DEGs) had already been well established. Despite these advantages, the strong hyperfine interaction with nuclear spins in GaAs limited spin coherence times, which motivated the exploration of isotopically controlled silicon (Si) quantum-dot qubits [8–11], where the absence of nuclear spins improves spin coherence. Furthermore, two-dimensional materials [12–16] have also been proposed as hosts for Kramers qubits [17], exploiting additional degrees of freedom such as valley states. These materials are expected to offer excellent qubit performance, particularly with respect to the coherence time of quantum states [18].

Zinc oxide (ZnO) is also considered a promising candidate for qubits that could achieve high performance regarding both long coherence times and efficient coupling to photons, advancing beyond current limitations in quantum device platforms. These advantages are supported by ZnO's unique material properties. One is its low density of nuclear spins (only 4% of naturally occurring Zn isotopes and 0.04% of O isotopes possess nuclear spin), which contributes to the potential for long coherence times [18–20]. Moreover, ZnO is a direct bandgap semiconductor [21], which is beneficial for efficient coupling with photons [22].

In addition to these properties, 2DEG formed in ZnO heterostructures exhibits a mobility comparable to that of conventional high-quality semiconductor materials [23, 24] which enables to form fine structures showing quantum transport characteristics. Quantum transport phenomena such as the quantum Hall effect [25–27], quantum point contacts [28], and notably quantum dots [29] have been experimentally reported in ZnO devices, leading to increasing research on quantum devices. However, qubit operation in ZnO remains challenging, as it requires the formation of few-electron states in quantum dots [1–3] and the development of high-speed qubit readout techniques.

Charge sensing using radio-frequency (rf) reflectometry addresses these challenges, as it is capable of detecting a single electron charge in few-electron states with a broad bandwidth [30–32]. Devices should satisfy some criteria to perform rf reflectometry, one of which is possessing minimal stray capacitance in the device structure [13, 33]. If device design, typically QPC width and/or gate electrode pitch, is not optimized, gate electric fields create depletion regions not only directly below gate electrodes but also in channel regions. Under such conditions, quantum dots tend to form before complete depletion occurs below the gate electrodes, resulting in unexpected capacitive coupling between the 2DEG and the gate electrodes. As a result, rf signals leak through this parasitic capacitance, bypassing the quantum dots.

In this perspective, the device design is a particular concern in the case of ZnO heterostructures due to their unique material parameters such as the relative permittivity $\varepsilon_{\mathrm{ZnO}} = 8.3$ and the effective mass $m_{\mathrm{ZnO}} = 0.3m_0$, where m_0 is the bare electron mass. [34, 35] These values are different from those of conventional materials such as $\varepsilon_{\mathrm{GaAs}} = 12.9$, $\varepsilon_{\mathrm{Si}} = 11.7$, $m_{\mathrm{GaAs}} = 0.067m_0$, and $m_{\mathrm{Si/SiGe}} = 0.22m_0$ [26]. These parameters may affect the pinch-off characteristics and the orbital level spacing. In fact, a previous experimental study reported abrupt changes in the tunnel coupling between quantum dots and leads as a function of gate voltage [29], which complicates device design for rf reflectometry. Thus, several open questions remain as to whether ZnO heterostructures can utilize device designs similar to those proven effective for GaAs and Si, or whether entirely new architectures are required for rf reflectometry of highly integrated qubit systems in the future.

In this paper, we fabricate a device structure using a ZnO heterostructure to form target and sensor quantum dots. The sensor dot is integrated into the resonator circuit to demonstrate rf reflectometry and provides a charge stability diagram of few-electron double quantum dots. We also present the first benchmark of the bandwidth, sensitivity, and readout fidelity of rf reflectometry in ZnO-based quantum dots.

II. RESULTS AND DISCUSSION

A. Charge detection

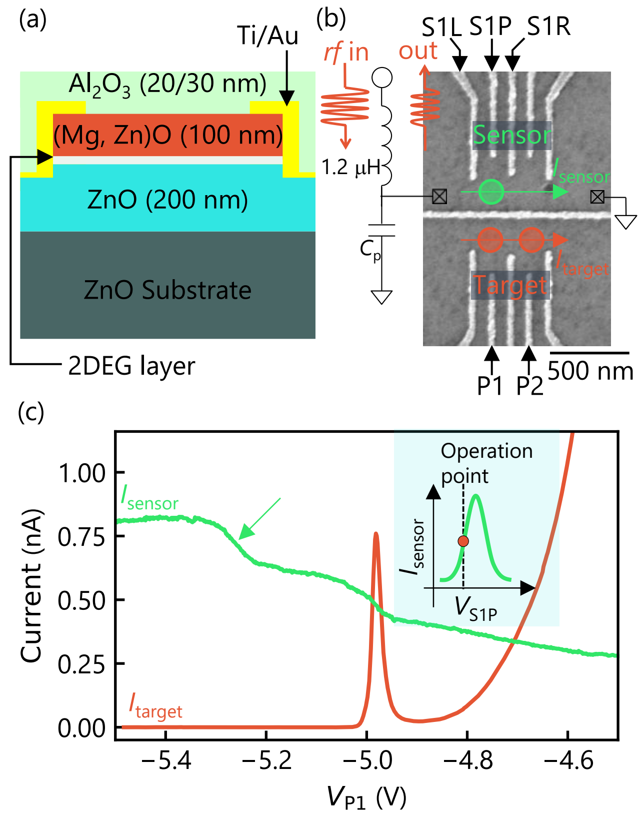

FIG. 1. (a) Schematic of the device structure. (b) Scanning electron microscope image of the fabricated device and the resonance circuit. (c) Gate voltage V_{P1} dependence of the sensor current I_{sensor} and target current I_{target}. The inset shows an operation point of the sensor dot.

The layer structure of the device is illustrated in Figure 1(a). The numbers in parentheses represent the layer thicknesses in nanometers. The 2DEG forms at the interface between the (Mg,Zn)O and ZnO heterostructure. We prepare two types of AlO_x gate insulator stack structures: one with a 20-nm AlO_x layer and another with a 30-nm layer. The latter structure is used for spin-state readout measurements.

Figure 1(b) shows a scanning electron microscope image of the device and the schematic resonator. The upper dots correspond to the charge sensor, while the bottom to the target quantum dots. This device design is suitable for qubits integration, which is employed in other material systems[36, 37]. As part of our design process, we optimize the QPC width to form quantum dots that avoid formation of the stray capacitance. The sensor quantum dot is embedded in an rf resonator circuit constructed with a 1.2 μH chip inductor and stray capacitance C_{p}. All experimental measurements are performed within a dilution refrigerator maintained at 60 mK.

To demonstrate the charge sensor operation, we measure two types of source-drain current: one through the sensor dot I_{sensor} and another through the target dot I_{target}. Figure 1(c) shows I_{sensor} and I_{target} as a function of the gate voltage V_{P1}, where the sensor's operating gate voltage V_{S1P} is set to the slope of the Coulomb peak as shown in the inset of Fig. 1c. I_{target} exhibits a typical Coulomb peak behavior, indicating the formation of a quantum dot. At the peak position of I_{target} around $V_{\mathrm{P1}} = -5.0$ V, the step-like variation of I_{sensor} reflects the increase or decrease of electrons in the target dot because the electron acts as an effective gate voltage on the sensor dot through the electrostatic coupling between the target and sensor dots. Note that V_{S1P} is compensated to maintain the operation point, as V_{P1} affects the sensor dot conductance. Another noticeable change in I_{sensor} is observed at $V_{\mathrm{P1}} \approx -5.25$ V (indicated by the arrow) while I_{target} remains nearly constant at zero. This is because, in this region, the tunnel couplings between the target dot and the lead electrodes are extremely weak, resulting in nearly zero current, even when an electron is added to the target dot. This behavior is also observed in the previous study in GaAs by using a quantum point contact sensor [31]. This condition corresponds to an upper limit on the tunneling rate of 1.1 MHz by considering our measurement resolution while Coulomb peak observed at $V_{\mathrm{P1}} = -5.0$ V corresponds to a tunneling rate of approximately 5 GHz by assuming sequential tunneling in the transport current measurement. These results demonstrate that the charge sensor enables accurate counting of the number of electrons in the target dot, even when the direct current through the target dot is too small to be detected.

B. Radio-frequency reflectometry

Next, we investigate the resonator properties to perform the rf reflectometry. The reflected signal from the resonator is measured using a network analyzer connected through a directional coupler as shown in Fig. 2(a). Figure 2(b) shows the transmission coefficients S_{21} as functions of frequency and V_{S1P}, while maintaining the gate voltages V_{S1R} and V_{S1L} at fixed values of -3.84 V and -4.42 V, respectively. Note that S_{21} is determined by measuring the input signal and the reflected signal from the resonator using a directional coupler, effectively representing the reflection coefficients. The resonance frequency is approximately 174 MHz, corresponding to C_{p} of 0.69 pF. We calculate the resonator Q factor to be approximately 15 by using the full width at half maximum of the resonant dip. The dip depth is modulated by V_{S1P}, reflecting the changes in conductance of the sensor dot, while the resonance frequency remains nearly constant suggesting that unexpected capacitance leading to rf signal leakage is suppressed. Figure 2(c) shows typical traces of S_{21}. At $V_{\mathrm{S1P}} = -4.32$ V, a pronounced dip is observed where the impedance matching condition is satisfied. In contrast, at $V_{\mathrm{S1P}} = -4.35$ V, a trace without impedance matching shows a small dip depth. This large variation in dip depth enables high-sensitivity charge sensing under matching conditions.

C. Few-electron quantum dots

Next, we switch the measurement setup to a demodulator circuit which is commonly used in rf reflectometry[31, 38]. Figure 3(a) illustrates the demodulator circuit for performing rf reflectometry. The resonator, which incorporates a charge sensor, receives the rf signal at a frequency of 174 MHz via a directional coupler. The amplitude of the rf signal is set to -93 dBm at the sample end. After reflection, this rf signal undergoes amplification and is then mixed with a local oscillator signal for demodulation. We optimize the phase shifter between the signal generator and the mixer. The resulting down-converted signal voltage, denoted as V_{rf}, is digitized. The sampling rate is set to 100 MHz. To find the operation point, we measure the frequency and V_{S1P} dependence of a numerical derivative $\mathrm{d}V_{\mathrm{rf}}/\mathrm{d}V_{\mathrm{S1P}}$, as illustrated in Figure 3(b). A phase difference between the reflected signal and the local oscillator at the mixer modulates V_{rf}. A typical additional phase is caused by a phase shift induced by the circuit line, whose effects appear as periodic changes on V_{rf} along the frequency axis. This color pattern, also observed in previous studies using GaAs and GaN quantum dots [38, 39], shows optimum operation points where the maximum sensitivity is obtained.

Figure 3(c) shows I_{sensor} and V_{rf} with sweeping V_{S1P}, where we perform an integration of 2×10^5 data points to reduce the noise in V_{rf}. The changes in V_{rf} and I_{sensor} are synchronized, allowing us to detect the change in I_{sensor} by monitoring V_{rf}. The region where V_{rf} approaches zero satisfies the impedance matching condition, enabling high sensitivity for rf charge sensing. After establishing the rf charge sensing technique, we apply this technique to probe the formation of double quantum dots in the target region. The charge stability diagram obtained by monitoring V_{rf} while sweeping V_{P1} and V_{P2} is shown in Fig. 3(d). Two distinct slopes in the charge transition lines indicate the formation of double quantum dots. The absence of charge transition lines in the more negative gate voltage region indicates the full depletion of the double quantum dot. By counting the number of electrons using the charge transition lines, we can assign the number of electrons in each region as shown in the figure. This result clearly shows we achieve few-electron states in this double quantum dot system.

In this section, we have demonstrated charge detection utilizing the sensor quantum dot and rf reflectometry, and observed few-electron double quantum dots in ZnO. The employed device design has the potential to integrate more quantum dots, suggesting that the ZnO quantum dots platform could also become a candidate for high-density qubit systems

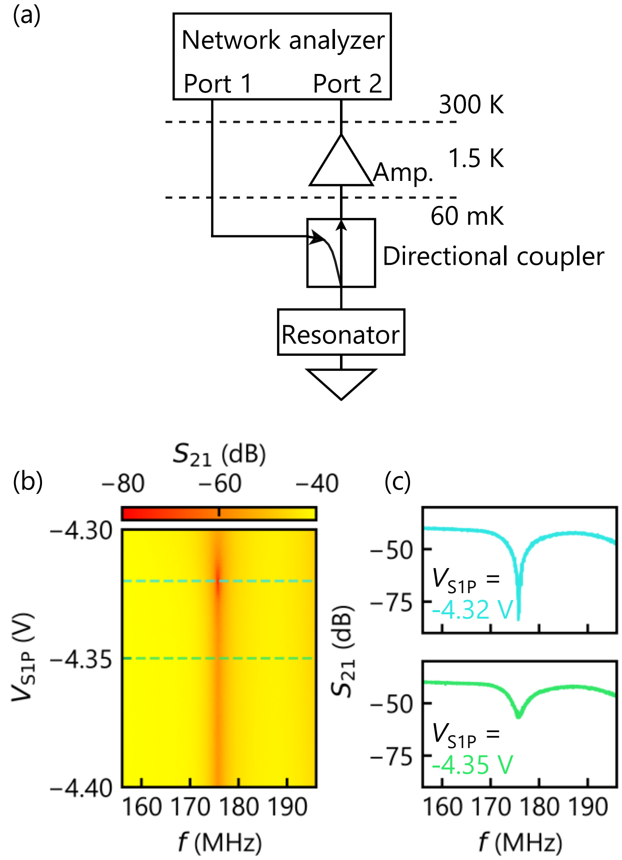

FIG. 2. (a) Measurement setup to evaluate the resonator properties. (b) V_{S1P} dependence of the resonator's S_{21} parameter. The color scale represents the magnitude of S_{21} in dB. (c) S_{21} characteristics showing typical traces with ($V_{\mathrm{S1P}} = -4.32$ V) and without ($V_{\mathrm{S1P}} = -4.35$ V) impedance matching.

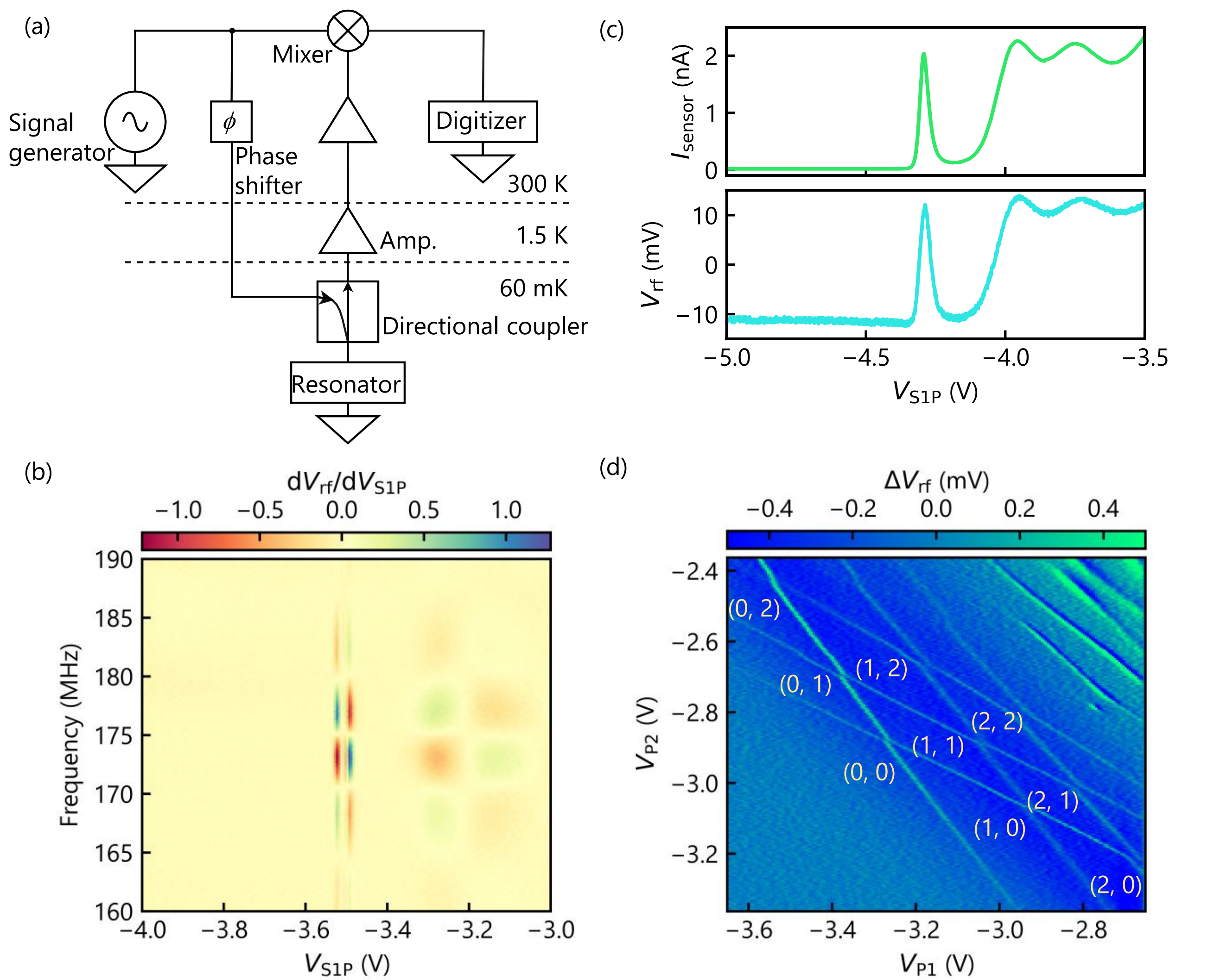

FIG. 3. (a) Schematic of the demodulator circuit. (b) Frequency and V_{S1P} dependence of $\mathrm{d}V_{\mathrm{rf}}/\mathrm{d}V_{\mathrm{S1P}}$. (c) I_{sensor} and V_{rf} as a function of V_{S1P}. (d) Charge stability diagram of a few electron double quantum dots probed by V_{rf}. ΔV_{rf} is the numerical difference in V_{rf} along the V_{P1} axis direction.

as well as Si systems. These are important steps toward realizing spin qubits utilizing ZnO and single-shot readout of the qubit states.

D. Charge sensitivity and error rate calculation

Here, we estimate the charge sensitivity of our measurement system. The noise σ_0, defined as the standard deviation of real-time measurement, is evaluated to be 36.8 mV. From the charge stability diagram shown in Fig. 3(d), we estimate effective gate-voltage shifts of the sensor dot for each single-electron transition in the target dots of (0,0) $\leftrightarrow$ (1,0), (0,0) $\leftrightarrow$ (0,1), and (1,0) $\leftrightarrow$ (0,1). The shifts for the (0,0) $\leftrightarrow$ (1,0) and (0,0) $\leftrightarrow$ (0,1) transitions are extracted to be 3.20 mV and 1.00 mV, respectively. This difference allows us to distinguish the charge states (1,0) and (0,1) which is important for observing the interdot charge transition in the spin blockade measurement. Note that the sensor dot is biased over a wide dynamic range to obtain such a wide stability diagram. Using these values together with the charge sensor slope extracted from Fig. 3(c), which corresponds to the most sensitive sensor condition, the detection voltages dV for each single-electron transition in the target dots of (0,0) $\leftrightarrow$ (1,0), (0,0) $\leftrightarrow$ (0,1), and (1,0) $\leftrightarrow$ (0,1) are estimated to be 2.19 mV, 0.69 mV and 1.51 mV, respectively. By using σ_0 and $\mathrm{d}V$, we find that time integration to reduce the noise determines measurement bandwidths f_{bw} of 178 kHz, 17.4 kHz and 84.2 kHz. These values are required to achieve $\mathrm{SNR} = 1$ defined by following equation,

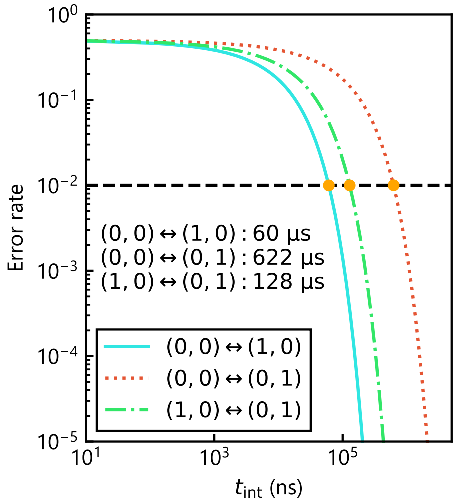

FIG. 4. Error rate for each single-electron transition in the target dots of (0,0) ↔ (1,0), (0,0) ↔ (0,1), and (1,0) ↔ (0,1) as a function of the integration time $t_{\rm int}$.

$$\mathrm{SNR} = \frac{\mathrm{d}V}{\sigma_0\sqrt{f_{\rm bw}/f_0}}. \quad (1)$$

Here, f_0 is the measurement bandwidth to evaluate σ_0. The charge sensitivities for three electron transitions are calculated to be 2.37×10^{-3} $\mathrm{eHz}^{-1/2}$, 7.58×10^{-3} $\mathrm{eHz}^{-1/2}$, and 3.45×10^{-3} $\mathrm{eHz}^{-1/2}$ by considering found value of each $f_{\rm bw}$. These values are consistent with the previous report using GaAs system [31].

We also estimate the potential error rate of single charge detection in the presented system by using the following equations [13]

$$\text{Error Rate} = 0.5\mathrm{erfc}\left(\frac{\mathrm{SNR}}{2\sqrt{2}}\right). \quad (2)$$

Figure 4 shows the calculated error rate as a function of an integration time $t_{\rm int} = \frac{1}{f_{\rm bw}}$. The orange points indicate that $t_{\rm int} \approx 60$ μs, 128 μs, and 622 μs satisfy the reading accuracy of 99% for each single-electron transition. These times are shorter than the longitudinal relaxation time T_1 reported for shallow donor qubits in ZnO [19]. Note that our gate-defined quantum dots differ from those donor systems in geometry and mechanisms. Experimentally establishing T_1 in these devices will thus be important for future work.

Furthermore, we examine the noise on $V_{\rm rf}$ using other ZnO devices and resonators while keeping the same rf-circuit components and transmission lines, as described in Appendix section. These measurements show similar noise levels, indicating that the dominant contribution to the noise on $V_{\rm rf}$ originates from the preamplifier, as previously discussed for GaAs systems [38].

III. CONCLUSION

In this study, we demonstrate the charge sensing and rf reflectometry of ZnO quantum dots. The sensor dot detects the charge state of the target dots, which has been difficult to determine when measuring the source-drain current of the target directly. Owing to the charge sensor with the integration suitable design, we observe the few-electron regime of a double quantum dot system probed by rf reflectometry, which is essential for utilizing these systems as future high-density qubits. The presented device and measurement setup enable charge sensing with a readout accuracy of 99% within an integration time ranging from 60 μs to 622 μs, which is comparable to values reported for GaAs and Si systems. We have addressed the challenges associated with realizing few-electron states and rf reflectometry in ZnO quantum dots, which are essential for their application as qubits. These results indicate that ZnO quantum devices can progress together with GaAs and Si devices by leveraging the technology developed for these material systems, paving the way for quantum information processing applications using ZnO quantum devices.

ACKNOWLEDGEMENTS

The authors thank K. Dezaki, M. Takeuchi, A. Kurita, and the RIEC Fundamental Technology Center and the Laboratory for Nanoelectronics and Spintronics for fruitful discussions and technical support. Part of this work was supported by MEXT Leading Initiative for Excellent Young Researchers, Grants-in-Aid for Scientific Research (21K18592, 22H04958, 23H01789, 23H04490), Tanigawa Foundation Research Grant, Maekawa Foundation Research Grant, The Foundation for Technology Promotion of Electronic Circuit Board, Iketani Science and Technology Foundation Research Grant, The Ebara Hatakeyama Memorial Foundation Research Grant, FRiD Tohoku University, and "Advanced Research Infrastructure for Materials and Nanotechnology in Japan (ARIM)" of the Ministry of Education, Culture, Sports, Science and Technology (MEXT) (Proposal Number JPMXP1224NM5072). AIMR and MANA are supported by World Premier International Research Center Initiative (WPI), MEXT, Japan.

COMPETING INTERESTS

The authors declare no competing interests.

APPENDIX A:NOISE EVALUATION WITH A DIFFERENT DEVICE AND RESONATOR CIRCUIT

We evaluate the charge sensitivity for a ZnO quantum dot device different from the device referred to in the main text. From the stability diagram shown in Fig. 5(a), we extract the effective gate-voltage shifts for each electron transitions (0,1) ↔ (0,2), (0,1) ↔ (1,1), and (1,1) ↔ (0,2) to be 5.15 mV, 3.61 mV, and 4.34 mV, respectively. The noise standard deviation with a 48 MHz low-pass filter is measured to be $\sigma_0 = 57.2$ mV. Using these parameters, the bandwidths for each electron transition are calculated to be 390 kHz, 191 kHz, and 277 kHz, corresponding to the charge sensitivities of 1.60×10^{-3} eHz$^{-1/2}$, 2.29×10^{-3} eHz$^{-1/2}$, and 1.90×10^{-3} eHz$^{-1/2}$, respectively. Furthermore, we also evaluate the noise for a different resonator circuit by using the device discussed in the main text. In this device, the resonator circuit including an inductor of 1.2 µH is connected to the sensor quantum dot side as shown in Fig. 1(b) while the target side uses an inductor of 1.0 µH. The noise standard deviation of each side is calculated to be 34.3 mV and 36.8 mV.

APPENDIX B:PERSPECTIVE FOR SPIN-BLOCKADE MEASUREMENTS

After the formation of few-electron double quantum dots, spin-state readout measurements are expected as the next step. In this appendix section, we provide a perspective on spin blockage measurements. For the spin blockade measurement [40, 41], we measure the stability diagram with a gate voltage pulse sequence under an in-plane magnetic field of 50 mT [32, 33, 42]. Here, the sampling rate is set to 125 MHz. We perform this measurement near the (0,2) to (1,1) charge transition, where (n_{P1}, n_{P2}) indicates the number of electrons in the quantum dots defined by V_{P1} and V_{P2}. At the reset pulse step R, the two-electron state is initialized to either a singlet or one of the three triplet states. If initialized to the singlet state, the state is transferred to the (0,2) charge state during the next measure pulse step M. Conversely, if initialized to one of the triplet states, it remains in the (1,1) charge state during this pulse M. After the measurement, one of the electrons is evacuated during the pulse step E to prepare the next reset phase. As a result, the signal from the (1,1) state is expected to appear in the region near the boundary between the (0,2) and (1,1) states, approximately within the dashed region in Fig. 5(a) [32, 33, 42]. However, the absence of signals in these regions indicates that spin blockade does not occur and/or the spin state might be relaxed by not fully optimized tunneling rates. Note that this measurement is performed in a different device with similar structures.

Because there are many possible reasons for the absence of spin blockade such as tuning of tunneling rates, it is difficult to determine the origin of the absence. Here, we discuss the effect of electron correlation in ZnO as one of the possible mechanisms. For a two-electron state, considering both orbital and spin degrees of freedom, the spin states almost degenerate in the low magnetic field. These spin states are represented as $|T^+\rangle = |\uparrow\rangle_1 |\uparrow\rangle_2$, $|T^0\rangle = \frac{1}{\sqrt{2}} (|\uparrow\rangle_1 |\downarrow\rangle_2 + |\downarrow\rangle_1 |\uparrow\rangle_2)$, $|T^-\rangle = |\downarrow\rangle_1 |\downarrow\rangle_2$, and $|S\rangle = \frac{1}{\sqrt{2}} (|\uparrow\rangle_1 |\downarrow\rangle_2 - |\downarrow\rangle_1 |\uparrow\rangle_2)$. As a result, the energy of the electronic state is determined by the orbital energy. Regarding the (0, 2) state, the orbital states for the ground (excited) spin-singlet $|\psi_S\rangle_{\mathrm{G}}$ ($|\psi_S\rangle_{\mathrm{E}}$) and triplet $|\psi_T\rangle$ configurations can be expressed as

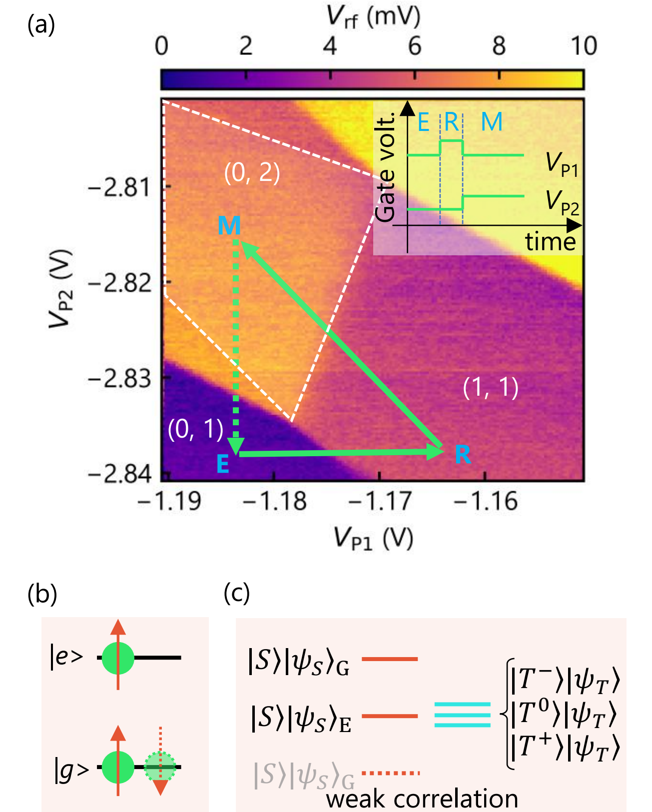

FIG. 5. (a) Charge stability diagram with a gate pulse sequence under an in-plane magnetic field of 50 mT. The inset indicates a three-step gate pulse sequence to observe the spin blockade. The dwell times of E, R, and M are 1000 ns, 600 ns, and 10000 ns, respectively. (b) Energy levels of the ground and excited orbital states. With strong electron correlation, the formation of the ground singlet is forbidden and the higher orbital is occupied by the second electron. (c) Energy levels of two-electron states considering both orbital and spin configurations with strong electron correlation. The dotted line indicates the ground state in the case of weak electron correlation.

$$
\begin{aligned}
|\psi_S\rangle_{\mathrm{G}} &= |g\rangle_1 |g\rangle_2 \,, \\
|\psi_S\rangle_{\mathrm{E}} &= \frac{1}{\sqrt{2}} \left(|g\rangle_1 |e\rangle_2 + |e\rangle_1 |g\rangle_2 \right) ,
\end{aligned}
\tag{3}
$$

$$
|\psi_T\rangle = \frac{1}{\sqrt{2}} \left(|g\rangle_1 |e\rangle_2 - |e\rangle_1 |g\rangle_2 \right) . \tag{4}
$$

Here, $|g\rangle$ and $|e\rangle$ are the ground and excited orbital states, as shown in Fig. 5(b). If the Coulomb interaction energy is larger than the difference between the ground and excited orbital levels, a second electron added to the quantum dot occupies the excited level. Under this condition, $|\psi_S\rangle_{\mathrm{E}}$ becomes the ground state, whereas in devices with weak electron correlation, such as GaAs, $|\psi_S\rangle_{\mathrm{G}}$ typically assumes this role. Consequently, even in the (0, 2) state, two-electron states with different spin configurations are nearly degenerate in energy, as shown in Fig. 5(c). This is in contrast to the usual scenario where only the singlet state forms the ground state $|S\rangle\,|\psi_S\rangle_{\mathrm{G}}$, enabling readout operations by spin-blockade. Indeed, the Kondo effect has been observed even in even-electron states in the ZnO quantum dot as a signature of strong electron correlation [29, 43]. Such behavior based on strong correlation supports the presented physical pictures, and our results suggest that improvements to the current situation or the establishment of new principles for readout methods are necessary. One possible approach to the first solution is fabricating devices with smaller designs, increasing the orbital energy spacing than the electron interaction.

DATA AVAILABILITY

The data that support the findings of this study are available in the article. Additional data related to this paper may be requested from the authors.

* tomohiro.otsuka@tohoku.ac.jp

[1] S. Tarucha, D. Austing, T. Honda, R. Van der Hage, and L. P. Kouwenhoven, Shell filling and spin effects in a few electron quantum dot, Phys. Rev. Lett. **77**, 3613 (1996).

[2] L. P. Kouwenhoven, T. Oosterkamp, M. Danoesastro, M. Eto, D. Austing, T. Honda, and S. Tarucha, Excitation spectra of circular, few-electron quantum dots, Science **278**, 1788 (1997).

[3] L. P. Kouwenhoven, D. Austing, and S. Tarucha, Few-electron quantum dots, Rep. Prog. Phys. **64**, 701 (2001).

[4] R. Maurand, X. Jehl, D. Kotekar-Patil, A. Corna, H. Bohuslavskyi, R. Laviéville, L. Hutin, S. Barraud, M. Vinet, M. Sanquer, and S. D. Franceschi, A CMOS silicon spin qubit, Nat. Commun. **7**, 13575 (2016).

[5] A. Zwerver, T. Krähenmann, T. Watson, L. Lampert, H. C. George, R. Pillarisetty, S. Bojarski, P. Amin, S. Amitonov, J. Boter, R. Caudillo, D. Correas-Serrano, J. P. Dehollain, G. Droulers, E. M. Henry, R. Kotlyar, M. Lodari, F. Lüthi, D. J. Michalak, B. K. Mueller, S. Neyens, J. Roberts, N. Samkharadze, G. Zheng, O. K. Zietz, G. Scappucci, M. Veldhorst, L. M. K. Vandersypen, and J. S. Clarke, Qubits made by advanced semiconductor manufacturing, Nat. Electron. **5**, 184 (2022).

[6] F. H. Koppens, C. Buizert, K.-J. Tielrooij, I. T. Vink, K. C. Nowack, T. Meunier, L. Kouwenhoven, and L. Vandersypen, Driven coherent oscillations of a single electron spin in a quantum dot, Nature **442**, 766 (2006).

[7] J. Yoneda, T. Otsuka, T. Nakajima, T. Takakura, T. Obata, M. Pioro-Ladrière, H. Lu, C. Palmstrøm, A. Gossard, and S. Tarucha, Fast electrical control of single electron spins in quantum dots with vanishing influence from nuclear spins, Phys. Rev. Lett. **113**, 267601 (2014).

[8] M. Fogarty, K. Chan, B. Hensen, W. Huang, T. Tanttu, C. Yang, A. Laucht, M. Veldhorst, F. Hudson, K. M. Itoh, D. Culcer, T. D. Ladd, A. Morello, and A. S. Dzurak, Integrated silicon qubit platform with single-spin addressability, exchange control and single-shot singlet-triplet readout, Nat. Commun. **9**, 4370 (2018).

[9] J. Yoneda, K. Takeda, T. Otsuka, T. Nakajima, M. R. Delbecq, G. Allison, T. Honda, T. Kodera, S. Oda, Y. Hoshi, N. Usami, K. M. Itoh, and S. Tarucha, A quantum-dot spin qubit with coherence limited by charge noise and fidelity higher than 99.9%, Nat. Nanotechnol. **13**, 102 (2018).

[10] K. Takeda, A. Noiri, T. Nakajima, T. Kobayashi, and S. Tarucha, Quantum error correction with silicon spin qubits, Nature **608**, 682 (2022).

[11] A. Noiri, K. Takeda, T. Nakajima, T. Kobayashi, A. Sammak, G. Scappucci, and S. Tarucha, Fast universal quantum gate above the fault-tolerance threshold in silicon, Nature **601**, 338 (2022).

[12] L. Banszerus, S. Möller, E. Icking, C. Steiner, D. Neumaier, M. Otto, K. Watanabe, T. Taniguchi, C. Volk, and C. Stampfer, Dispersive sensing of charge states in a bilayer graphene quantum dot, Appl. Phys. Lett. **118**, 093104 (2021).

[13] T. Johmen, M. Shinozaki, Y. Fujiwara, T. Aizawa, and T. Otsuka, Radio-Frequency Reflectometry in Bilayer Graphene Devices Utilizing Microscale Graphite Back-Gates, Phys. Rev. Appl. **20**, 014035 (2023).

[14] R. Garreis, C. Tong, J. Terle, M. J. Ruckriegel, J. D. Gerber, L. M. Gächter, K. Watanabe, T. Taniguchi, T. Ihn, K. Ensslin, and W. W. Huang, Long-lived valley states in bilayer graphene quantum dots, Nat. Phys. **20**, 428 (2024).

[15] R. Tataka, A. Sharma, M. Shinozaki, T. Johmen, T. Kumasaka, Y. P. Chen, and T. Otsuka, Surface Gate-Defined Quantum Dots in MoS_2 with Bi Contacts, J. Phys. Soc. Jpn. **93**, 094601 (2024).

[16] M. J. Ruckriegel, L. M. Gächter, D. Kealhofer, M. Bahrami Panah, C. Tong, C. Adam, M. Masseroni, H. Duprez, R. Garreis, K. Watanabe, T. Taniguchi, A. Wallraff, T. Ihn, K. Ensslin, and W. W. Huang, Electric Dipole Coupling of a Bilayer Graphene Quantum Dot to a High-Impedance Microwave Resonator, Nano Lett. **24**, 7508 (2024).

[17] A. O. Denisov, V. Reckova, S. Cances, M. J. Ruckriegel, M. Masseroni, C. Adam, C. Tong, J. D. Gerber, W. W. Huang, K. Watanabe, T. Taniguchi, T. Ihn, K. Ensslin, and H. Duprez, Spin–valley protected Kramers pair in bilayer graphene, Nat. Nanotechnol. **20**, 494 (2025).

[18] S. Kanai, F. J. Heremans, H. Seo, G. Wolfowicz, C. P. Anderson, S. E. Sullivan, M. Onizhuk, G. Galli, D. D. Awschalom, and H. Ohno, Generalized scaling of spin qubit coherence in over 12,000 host materials, Proceedings of the National Academy of Sciences **119**, e2121808119 (2022).

[19] X. Linpeng, M. L. Viitaniemi, A. Vishnuradhan, Y. Kozuka, C. Johnson, M. Kawasaki, and K.-M. C. Fu, Coherence properties of shallow donor qubits in ZnO, Phys. Rev. Appl. **10**, 064061 (2018).

[20] V. Niaouris, M. V. Durnev, X. Linpeng, M. L. K. Viitaniemi, C. Zimmermann, A. Vishnuradhan, Y. Kozuka, M. Kawasaki, and K.-M. C. Fu, Ensemble spin relaxation of shallow donor qubits in ZnO, Phys. Rev. B **105**, 195202 (2022).

[21] A. Tsukazaki, M. Kubota, A. Ohtomo, T. Onuma, K. Ohtani, H. Ohno, S. F. Chichibu, and M. Kawasaki, Blue light-emitting diode based on ZnO, Jpn. J. Appl. Phys. **44**, L643 (2005).

[22] J.-Y. Yan, C. Chen, X.-D. Zhang, Y.-T. Wang, H.-G. Babin, A. D. Wieck, A. Ludwig, Y. Meng, X. Hu, H. Duan, W. Chen, W. Fang, M. Cygorek, X. Lin, D.-W. Wang, C.-Y. Jin, and F. Liu, Coherent control of a high-orbital hole in a semiconductor quantum dot, Nat. Nanotechnol. **18**, 1139 (2023).

[23] J. Falson, Y. Kozuka, J. H. Smet, T. Arima, A. Tsukazaki, and M. Kawasaki, Electron scattering times in ZnO based polar heterostructures, Appl. Phys. Lett. **107**, 082102 (2015).
[24] J. Falson, Y. Kozuka, M. Uchida, J. H. Smet, T.-h. Arima, A. Tsukazaki, and M. Kawasaki, MgZnO/ZnO heterostructures with electron mobility exceeding 1×10^6 cm^2/Vs, Sci. Rep. **6**, 26598 (2016).
[25] A. Tsukazaki, A. Ohtomo, T. Kita, Y. Ohno, H. Ohno, and M. Kawasaki, Quantum hall effect in polar oxide heterostructures, Science **315**, 1388 (2007).
[26] A. Tsukazaki, S. Akasaka, K. Nakahara, Y. Ohno, H. Ohno, D. Maryenko, A. Ohtomo, and M. Kawasaki, Observation of the fractional quantum hall effect in an oxide, Nat. Mater. **9**, 889 (2010).
[27] J. Falson, D. Maryenko, B. Friess, D. Zhang, Y. Kozuka, A. Tsukazaki, J. Smet, and M. Kawasaki, Even-denominator fractional quantum Hall physics in ZnO, Nat. Phys. **11**, 347 (2015).
[28] H. Hou, Y. Kozuka, J.-W. Liao, L. Smith, D. Kos, J. Griffiths, J. Falson, A. Tsukazaki, M. Kawasaki, and C. Ford, Quantized conductance of one-dimensional strongly correlated electrons in an oxide heterostructure, Phys. Rev. B **99**, 121302 (2019).
[29] K. Noro, Y. Kozuka, K. Matsumura, T. Kumasaka, Y. Fujiwara, A. Tsukazaki, M. Kawasaki, and T. Otsuka, Parity-independent Kondo effect of correlated electrons in electrostatically defined ZnO quantum dots, Nat. Commun. **15**, 9556 (2024).
[30] H. Qin and D. A. Williams, Radio-frequency point-contact electrometer, Appl. Phys. Lett. **88**, 203506 (2006).
[31] D. Reilly, C. Marcus, M. Hanson, and A. Gossard, Fast single-charge sensing with a rf quantum point contact, Appl. Phys. Lett. **91**, 162101 (2007).
[32] C. Barthel, D. Reilly, C. M. Marcus, M. Hanson, and A. Gossard, Rapid single-shot measurement of a singlet-triplet qubit, Phys. Rev. Lett. **103**, 160503 (2009).
[33] A. Noiri, K. Takeda, J. Yoneda, T. Nakajima, T. Kodera, and S. Tarucha, Radio-frequency-detected fast charge sensing in undoped silicon quantum dots, Nano Lett. **20**, 947 (2020).
[34] Y. Kozuka, A. Tsukazaki, and M. Kawasaki, Challenges and opportunities of ZnO-related single crystalline heterostructures, Applied Physics Reviews **1**, 011303 (2014).
[35] Y. Kasahara, Y. Oshima, J. Falson, Y. Kozuka, A. Tsukazaki, M. Kawasaki, and Y. Iwasa, Correlation-Enhanced Effective Mass of Two-Dimensional Electrons in $\mathrm{Mg}_x\mathrm{Zn}_{1-x}\mathrm{O/ZnO}$ Heterostructures, Phys. Rev. Lett. **109**, 246401 (2012).
[36] T. Ito, T. Otsuka, S. Amaha, M. R. Delbecq, T. Nakajima, J. Yoneda, K. Takeda, G. Allison, A. Noiri, K. Kawasaki, and S. Tarucha, Detection and control of charge states in a quintuple quantum dot, Sci. Rep. **6**, 39113 (2016).
[37] H. C. George, M. T. Mądzik, E. M. Henry, A. J. Wagner, M. M. Islam, F. Borjans, E. J. Connors, J. Corrigan, M. Curry, M. K. Harper, D. Keith, L. Lampert, F. Luthi, F. A. Mohiyaddin, S. Murcia, R. Nair, R. Nahm, A. Nethwewala, S. Neyens, B. Patra, R. D. Raharjo, C. Rogan, R. Savytskyy, T. F. Watson, J. Ziegler, O. K. Zietz, S. Pellerano, R. Pillarisetty, N. C. Bishop, S. A. Bojarski, J. Roberts, and J. S. Clarke, 12-Spin-Qubit Arrays Fabricated on a 300 mm Semiconductor Manufacturing Line, Nano Lett. **25**, 793 (2025).
[38] M. Shinozaki, Y. Muto, T. Kitada, T. Nakajima, M. R. Delbecq, J. Yoneda, K. Takeda, A. Noiri, T. Ito, A. Ludwig, A. D. Dieck, S. Tarucha, and T. Otsuka, Gate voltage dependence of noise distribution in radio-frequency reflectometry in gallium arsenide quantum dots, Appl. Phys. Express **14**, 035002 (2021).
[39] Y. Fujiwara, M. Shinozaki, K. Matsumura, K. Noro, R. Tataka, S. Sato, T. Kumasaka, and T. Otsuka, Wide dynamic range charge sensor operation by high-speed feedback control of radio-frequency reflectometry, Appl. Phys. Lett. **123**, 213502 (2023).
[40] K. Ono, D. Austing, Y. Tokura, and S. Tarucha, Current rectification by pauli exclusion in a weakly coupled double quantum dot system, Science **297**, 1313 (2002).
[41] F. H. Koppens, J. A. Folk, J. M. Elzerman, R. Hanson, L. W. Van Beveren, I. T. Vink, H.-P. Tranitz, W. Wegscheider, L. P. Kouwenhoven, and L. M. Vandersypen, Control and detection of singlet-triplet mixing in a random nuclear field, Science **309**, 1346 (2005).
[42] A. Johnson, J. Petta, J. Taylor, A. Yacoby, M. Lukin, C. Marcus, M. Hanson, and A. Gossard, Triplet–singlet spin relaxation via nuclei in a double quantum dot, Nature **435**, 925 (2005).
[43] D. Maryenko, M. Kawamura, A. Ernst, V. Dugaev, E. Y. Sherman, M. Kriener, M. Bahramy, Y. Kozuka, and M. Kawasaki, Interplay of spin–orbit coupling and Coulomb interaction in ZnO-based electron system, Nat. Commun. **12**, 3180 (2021).